Run15 single diffractive EM-jet A_N analysis note

Xilin Liang

April 2, 2024

Contents

List of Figures

List of Tables

Chapter 1

Introduction

Transverse single-spin asymmetries (A_N), which are defined as left-right asymmetries of the particle production with respect to the plane defined by the momentum and spin directions of the polarized beam, have been observed to be large for charged- and neutral-hadron production in hadron-hadron collisions over a couple of decades [1, 2, 3, 4, 5]. In pQCD, however, the A_N is predicted to be small and close to zero in high energy collisions [6]. There are two major frameworks that can provide a potential explanation for such sizeable asymmetries. The first one is the transverse-momentum-dependent (TMD) contributions from the initial-state quark and gluon Sivers functions and/or the final-state Collins fragmentation functions. In the Sivers mechanism, the asymmetry comes from the correlation between the proton spin and the parton transverse momentum [7], while the Collins effect arises from the correlation between the spin of the fragmenting quark and the outgoing hadron's transverse momentum [8]. Another framework is based on the twist-3 contributions in the collinear factorization framework, including the quark-gluon or gluon-gluon correlations and fragmentation functions [9].

According to the study by CMS Collaboration [10], diffractive interactions contribute to about a significant fraction ($\sim$ 25%) of the total inelastic p+p cross section at high energies. The simulation for hard diffractive events based on PYTHIA-8 predicts that the fraction of diffractive cross section in the total inclusive cross section at the forward region is about 20% [4]. In recent years, analyses of A_N for forward π^0 and electromagnetic jets (EM-jets) in $p^{\uparrow} + p$ collisions at STAR indicated that there might be non-trivial contributions to the large A_N from diffractive processes [5, 11]. Measuring the A_N of diffractive process will provide an opportunity to study the properties and understand the diffractive exchange in p+p collisions.

Chapter 2

Dataset and Quality Assurance (QA)

2.1 General information for the dataset

The single diffractive EM-jet A_N analyses utilize polarized p+p collision at $\sqrt{s} = 200$ GeV taken in run 15. Details of the data set are listed as follow:

- Trigger setup name: production_pp200trans_2015
- Data stream: fms
- Production tag: P15ik
- File type: MuDst files in Distributed Disk (DD)

The analysis generates smaller size data stream files (NanoDst) from the MuDst files, applying trigger filter (described in Sec. (2.2)) and jet reconstruction (described in Sec. 3.1). In addition, the events with at least one Roman Pot track are required for diffractive EM-jet A_N analysis when generating the DST files.

2.2 Triggers

9 triggers for FMS are used for this analysis. The triggers with their ID are listed in Table (2.1). However, the FMS-sm-bs3 trigger is also considered a source of background. Therefore, the effect of this trigger will be studied as systematic uncertainty, which will be explained in 7.3.

Table 2.1: Trigger name lists and trigger ID for run 15

Trigger name	Trigger ID
FMS-JP0	480810 / 480830
FMS-JP1	480809 / 480829
FMS-JP2	480808 / 480828
FMS-sm-bs1	480801 / 480821 / 480841
FMS-sm-bs2	480802 / 480822
FMS-sm-bs3	480803 / 480823 / 480843
FMS-lg-bs1	480804 / 480824 / 480844
FMS-lg-bs2	480805 / 480825
FMS-lg-bs3	480806 / 480826

2.3 Calibration

The calibration for run 15 FMS dataset are from existing STAR framework [12], but with some additional steps. They mainly include the following items:

- Bit shift (BS): It refers to the binary bit, used to store the ADC value, not starting from the normal lowest bit. The BS will affect a cell's ADC distribution and the corresponding hit energy. The approach to check the BS is to use the ADC of each FMS hit to check with its corresponding BS value of the cell [12].

- Gain and gain correction: The energy of the hit = ADC $\times$ gain $\times$ gain correction. The gain is the calculated value based on a cell's η position, while the gain correction is obtained from offline calibration [12]. The flag of the gain and the gain correction for each tower in the STAR database is "fmsGainCorr-BNL-C".

- Hot channel and bad channel masking: A hot channel refers to the tower with a number of hits far more than the average number of hits for the whole detector towers within some time range. A bad channel refers to the problematic towers that might suffer from hardware issues. Both hot channels and bad channels can affect the quality of the calibration and the analyses since there are quite a lot of not physical signals contaminated. To mask out these channels, the gain values are set to zero. In addition to the

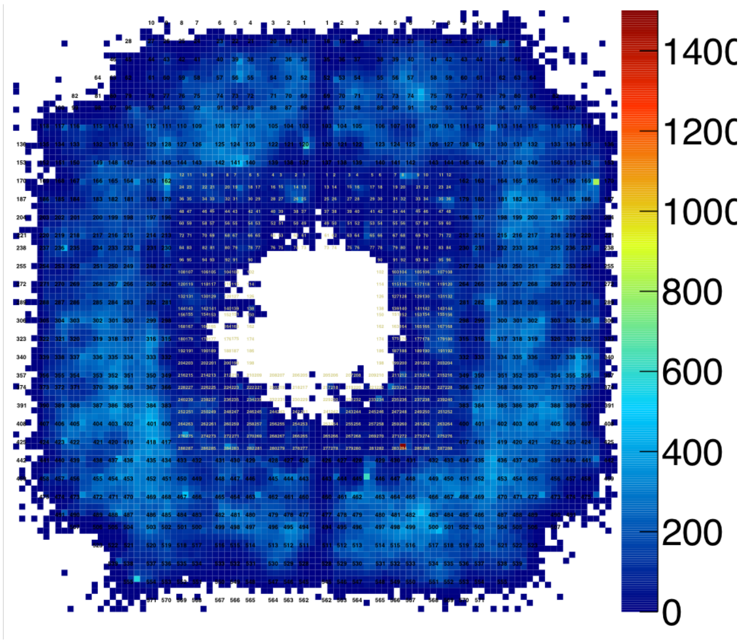

Figure 2.1: Example of EM-jet distribution at FMS before additional hot channel masking. The red color area in this plot indicates the possible hot channels.

existing hot channel and bad channel masking from STAR calibration [12], the fill-by-fill hot channel masking is applied in this analysis. The EM-jet distribution before any event selections for every fill is checked to find out any possible hot channels. The EM-jet reconstruction is discussed in 3.1. Figure (2.1) shows one example of the EM-jet distribution at the FMS. The areas with extremely high EM-jet entries compared to the overall average entries in the plot are assumed to be the hot channel area. The channels within these areas are considered hot channels and added manually to the hot channel lists. Figure (2.2) shows the EM-jet distribution for fill 18827 as an example after the additional hot channel masking. From the plot, the hot channels disappear, and the entries of the majority of towers are close to the average entries.

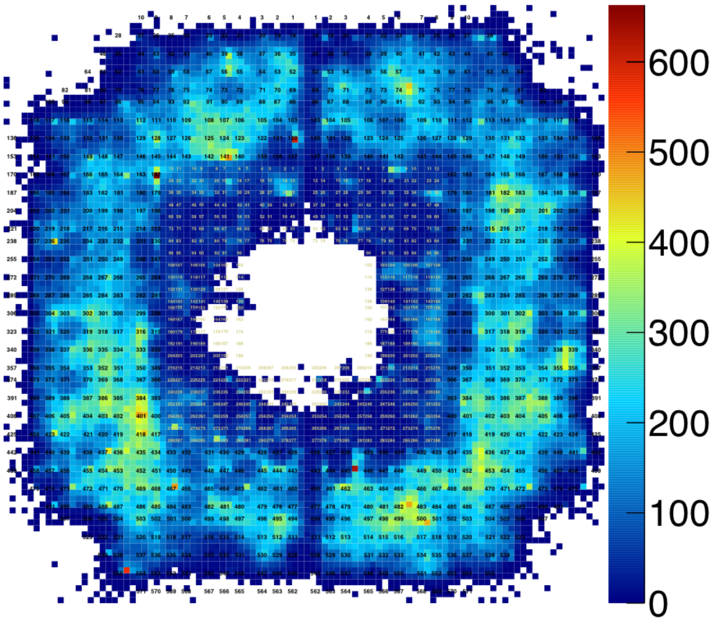

Figure 2.2: Example of EM-jet distribution at FMS after additional hot channel masking.

Chapter 3

Single Diffractive Process and Event Selection

One of the major characteristics of the diffractive processes is the presence of the rapidity gap. This analysis utilizes the proton track from east RP and the EM-jet at FMS, which allows for the large rapidity gap. Since there is only 1 proton in the final state process, this diffractive process is called the single diffractive process. The diagram for this process is shown in Fig. (3.1).

In order to determine the single diffractive process and minimize the effect of accidental coincidence events (AC) and pile-up events, the event selections and corrections include the following items:

1. Triggers: The triggers used for this analysis are the FMS BS triggers and FMS JP triggers. They are listed in Table(2.1). Only the events with any triggers fired are kept.

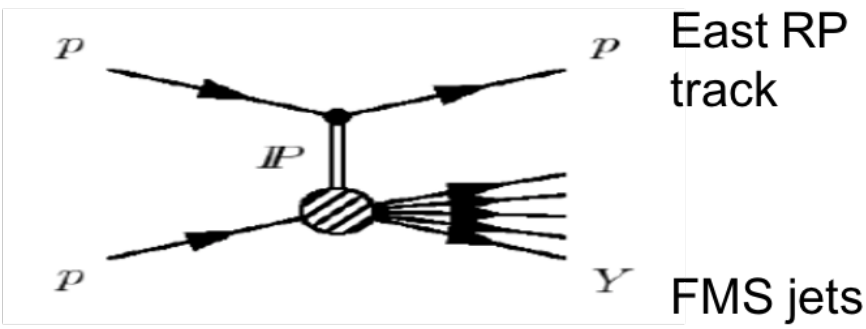

Figure 3.1: Diagram for single diffractive process.

2. EM-jet cut: Details of the EM-jet cuts are in Section (3.1)

   - EM-jet reconstruction: EM-jets are reconstructed by FMS points using the Anti-k_T algorithm with R = 0.7. The FMS points are required to have $E > 1$ GeV and $E_T > 0.2$ GeV.
   - The EM-jets are required to have $p_T > 2$ GeV and pass trigger p_T threshold.
   - The pseudorapidity (η) of the EM-jets is within [2.8, 3.8].
   - The event with EM-jet $E > 100$ GeV are excluded.
   - The number of EM-jets for each event is 1.
   - Energy corrections for EM-jets: Underlying-Event (UE) correction (details in Sector(4.1) , and EM-jet energy correction (details in Sector(4.2)))

3. Event property cut: Details of the event property cuts are in Section (3.2)

   - Veto on abort gap.
   - The spin status for the blue beam and yellow beam is correct and accepts the 4 cases of 4-bit spin patterns (Tab. (3.2)).
   - The vertex z is within [-80, 80] cm.

4. BBC East veto cut: Details of the BBC East veto cut are in Section (3.3).

   - East BBC ADC sum cut: east side large BBC ADC sum < 80 and east side small BBC ADC sum < 90.

5. Roman Pot (RP) track cut: Details are in Section (3.4)

   - Only accept the event with exactly only one east side RP track.
   - The east RP track must hit at least 7 RP silicon planes.
   - East RP track ξ dependent θ_X, θ_Y, p_X and p_Y cuts.
   - East RP track ξ range: $0 < \xi < 0.15$

3.1 Electromagnetic jet reconstruction and cuts

Electromagnetic jets (EM-jets) are jets consisting of only photons. The photon candidates for EM-jets reconstruction are the FMS points. The description of FMS points can be found in [14].

In order to reduce the noise background, only the FMS points with $E > 1$ GeV and $E_T > 0.2$ GeV are applied to the EM-jet reconstruction. The EM-jets are reconstructed with the anti-k_T algorithm from the FastJet package [13],

Trigger name	Trigger ID	15% increase p_T cut [GeV]
FMS-JP0	480810 / 480830	1.84
FMS-JP1	480809 / 480829	2.76
FMS-JP2	480808 / 480828	3.68
FMS-sm-bs1	480801	1.26
FMS-sm-bs1	480821 / 480841	1.15
FMS-sm-bs2	480802 / 480822	1.84
FMS-sm-bs3	480803	2.53
FMS-sm-bs3	480823 / 480843	2.18
FMS-lg-bs1	480804	1.26
FMS-lg-bs1	480824 / 480844	1.15
FMS-lg-bs2	480405 / 480425	1.84
FMS-lg-bs3	480406 / 480426	2.76

Table 3.1: EM-jet trigger threshold p_T cut, listed by trigger name and trigger ID.

with the resolution parameter $R = 0.7$. The primary vertex of the EM-jets is determined according to the priority of the TPC vertex, BBC vertex, and VPD vertex. If the primary vertex cannot be determined among these three detectors, it will be set to be (0,0,0). The EM-jet transverse momentum (p_T) is required to pass the trigger threshold and the fixed threshold 2 GeV/c threshold. The trigger thresholds are listed in Table (3.1). All of them have a 15% increase compared to the original trigger threshold setup.

The EM-jet vertex is determined by the primary vertex following the priority of TPC, BBC, and VPD. If the primary vertex can be obtained by TPC, the TPC vertex will be the primary vertex. Otherwise, check the BBC vertex on the next step. If there is no BBC vertex, then check the VPD vertex. If there is still no VPD vertex, the primary vertex is set to be z=0. The vertex z cut on $|z| < 80$ cm is considered.

In addition, we apply the cut on EM-jet pseudorapidity (η), which aims to get rid of the badly reconstructed EM-jets and the EM-jets hitting outside the FMS. Therefore, the η of the EM-jet cut is required to be within [2.8, 3.8].

Also, the events with EM-jet energy $E > 100$ GeV or $|x_F| > 1$ are discarded, where Feynman-x x_F can be estimated by the EM-jet energy divided by the beam energy ($x_F = \frac{2E}{\sqrt{s}}$). Those events with these unreasonable EM-jets are possibly pile-up events.

Finally, the number of EM-jets in each event is required to be only one. This can satisfy the requirement for single diffractive events and minimize the effect of the pile-up events.

Table 3.2: 4 acceptable 4-bit spin patterns

4-bit spin	Translate	Blue beam polarization	Yellow beam polarization
0101	5	up	up
0110	6	up	down
1001	9	down	up
1010	10	down	down

3.2 Event property cut

The abort gap for both blue beam and yellow beam is within bunch ID [31, 39] and [111, 119] for run 15. The events with either blue beam or yellow beam with the abort gap are discarded.

The spin patterns for each beam, either up or down, are obtained from the bunch crossing of each event. The translation from the database for the spin patterns is described in Tab. (3.2). The spin patterns for both blue and yellow beam are combined as 4-spin bit. The events satisfying the following 4 4-spin bit cases in Table (3.2) are considered in this analysis. These patterns require the polarizations of both blue and yellow beam are either up or down.

3.3 BBC East veto cut

The major goal for the BBC East veto cut is to minimize accidental coincidence events (AC), also called multiple collision events. It also helps to ensure the rapidity gap requirement for the diffractive process since the BBC East detector covers $-5 < \eta < -2.2$.

The study of BBC East veto cuts is carried out simultaneously with the East RP track cut study. To begin with, the rough cut on a small BBC East ADC sum < 150 is applied to get rid of some of the backgrounds because the events with high BBC East ADC sum are more likely to be AC events. Then, with the rough BBC East ADC sum cut, the East RP θ_X and θ_Y distributions for East RP track with different ξ ranges are checked, where ξ is the fraction of proton momentum loss in the collision. The goal of checking the rough East RP θ_X and θ_Y distributions is to figure out the rough East RP θ_X and θ_Y cuts and use them to further checking the proper small/large BBC East ADC sum distribution to determine the BBC East veto cuts. Figure (3.2) shows the rough East RP θ_X and θ_Y distributions for 7 different East RP ξ regions. From the hot areas for every single figure, which are shown in red and yellow color, we determine the rough cut for East RP θ_X and θ_Y. The rough East RP θ_Y cuts are: $2.0 < |\theta_Y| < 4.0 mrad$, and The rough East RP θ_X cuts are shown in Tab. (3.3). Then, with the rough East RP θ_X and θ_Y cuts applied, we

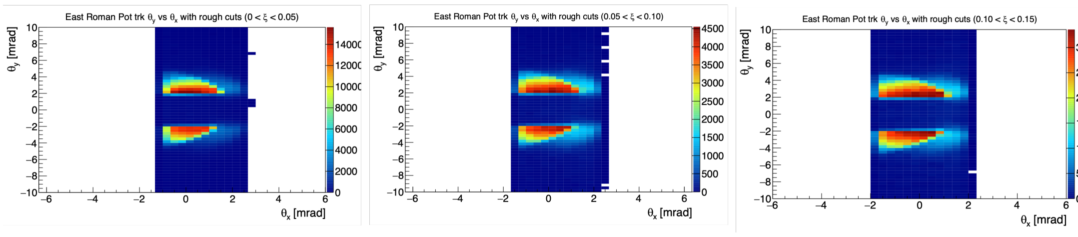

Figure 3.2: East RP θ_X and θ_Y distributions for 7 different East RP track ξ ranges with only applying East BBC ADC sum < 150.

ξ range	θ_X rough cuts [mrad]
$0.00 < \xi < 0.05$	$-1.0 < \theta_X < 1.5$
$0.05 < \xi < 0.10$	$-1.25 < \theta_X < 1.25$
$0.10 < \xi < 0.15$	$-1.5 < \theta_X < 1.25$
$0.15 < \xi < 0.20$	$-2.0 < \theta_X < 0.75$
$0.20 < \xi < 0.25$	$-2.5 < \theta_X < 0.75$
$0.25 < \xi < 0.30$	$-3.0 < \theta_X < 0.5$
$0.30 < \xi < 0.50$	$-5.0 < \theta_X < -0.25$

Table 3.3: Rough cuts for East RP track θ_X by different East RP track ξ

explore the small/large east BBC ADC sum distributions to determine the cuts on small/large east BBC cuts. The left panel of Fig. (3.3) shows the small east BBC ADC sum distribution, while the right panel of Fig. (3.3) shows the large east BBC ADC sum distribution. According to Fig. (3.3), we decide the small BBC east ADC sum < 90 and the large BBC east ADC sum < 80.

3.4 Roman Pot track cut

The proton track is detected from the RP detector, where the description of the RP detector can be found in [15]. For this analysis, we only accept the case with only one East RP track detected. To ensure the RP track is well reconstructed, the RP track must hit at least 7 RP silicon planes. Also, the BBC East veto cuts (details in Sec. (3.3)) are also applied to explore the East RP track cuts. Furthermore, according to the Particle Data Book [16], the proton ξ for the diffractive process should be less than 0.15. Therefore, the cut on East RP track $0 < \xi < 0.15$ is also applied. With all of these cuts applied, first of all,

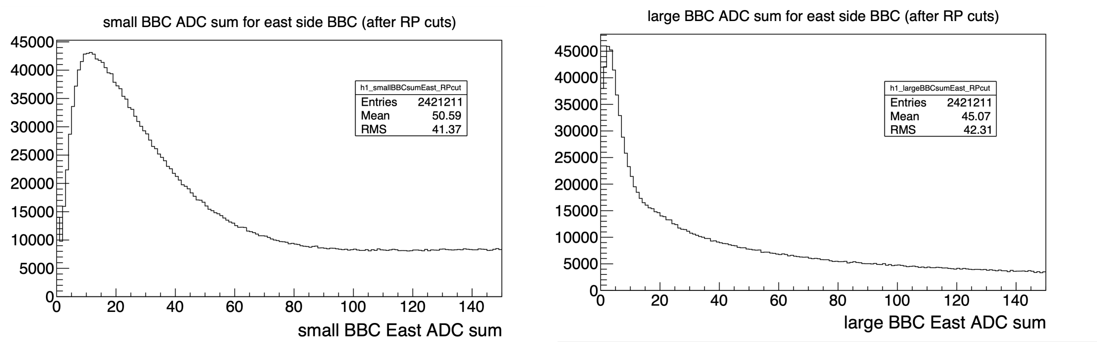

Figure 3.3: The small (left) and large (right) East BBC ADC sum distribution after the rough East RP θ_X and θ_Y cuts

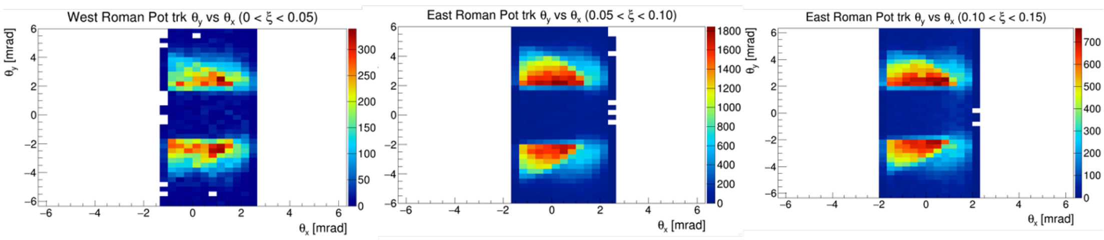

Figure 3.4: East RP θ_X and θ_Y distributions for three East RP track ξ ranges.

the East RP track θ_X and θ_Y distributions are further explored. Figure (3.4) shows the East RP track θ_X and θ_Y distributions for three ξ ranges. The hot area will be considered as acceptable final East RP θ_X and θ_Y cuts. The final East RP track θ_Y cuts are uniform for all three ξ ranges: $2 < |\theta_Y| < 4mrad$. However, the final East RP track θ_X cuts are ξ dependent, shown in Tab. (3.4). Finally, with then the final East RP θ_X and θ_Y cuts applied, the East RP track p_X and p_Y distributions are also explored to study their cuts. The idea is the same as investigating the East RP track θ_X and θ_Y cuts. Figure (3.5) shows the East RP track p_X and p_Y distributions for three ξ ranges. The shape of a rectangle with a quarter circle is used to describe the final East RP track p_X and p_Y cuts. The expressions are detailed in Tab. (3.5).

In summary, the cuts on East RP track include all the following: Number of RP Silicon planes hits greater than 6; $0 < \xi < 0.15$; East RP track θ_X and θ_Y cuts; East RP track p_X and p_Y cuts.

ξ range	θ_X final cuts [mrad]
$0.00 < \xi < 0.05$	$-1.0 < \theta_X < 1.5$
$0.05 < \xi < 0.10$	$-1.25 < \theta_X < 1.25$
$0.10 < \xi < 0.15$	$-1.5 < \theta_X < 1.25$

Table 3.4: Final cuts for East RP track θ_X by three ξ regions

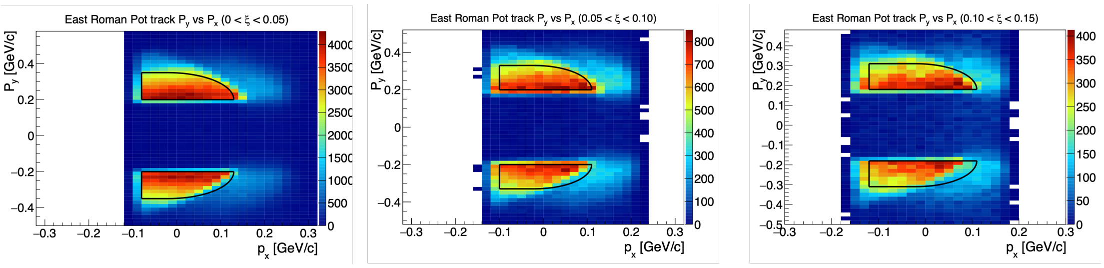

Figure 3.5: East RP track p_X and p_Y distributions for three East RP track ξ ranges. The black curves indicate the ranges of accepted East RP track p_X and p_Y cuts.

ξ range	p_X and p_Y final cuts [GeV/c]
$0.00 < \xi < 0.05$	$(p_X + 0.02)^2 + (\lvert p_Y\rvert - 0.2)^2 < 0.15^2$ or $-0.08 < p_X < -0.02$ and $0.2 < \lvert p_Y\rvert < 0.35$
$0.05 < \xi < 0.10$	$(p_X + 0.02)^2 + (\lvert p_Y\rvert - 0.2)^2 < 0.13^2$ or $-0.10 < p_X < -0.02$ and $0.2 < \lvert p_Y\rvert < 0.33$
$0.10 < \xi < 0.15$	$(p_X + 0.02)^2 + (\lvert p_Y\rvert - 0.18)^2 < 0.13^2$ or $-0.12 < p_X < -0.02$ and $0.18 < \lvert p_Y\rvert < 0.31$

Table 3.5: East RP track p_X and p_Y final cuts

Chapter 4

Corrections

4.1 Underlying Event (UE) correction

The underlying event contribution is part of a jet, not from the parton fragmentation but from secondary scattering or other processes. This will deposit some energy into the jet, so the correction on UE is required to subtract its energy from the jet. The commonly used method is the "off-axis" method [17]. In this method, first of all, two off-axis jets with the same pseudorapidity but at $\pm 1/2\pi$ azimuthal angle at the edge of the original jet are reconstructed as UE background. Then, the UE energy density (ρ) can be calculated using $\rho = E/(\pi R^2)$, where E is the UE energy and R is the UE jet radius. The fastjet program uses the "ghost particle" technique to calculate the jet area (A). The maximum "ghost particle" η is 5.0, and the "ghost area" is 0.04. Finally, the jet energy will be subtracted by the UE energy: $E_{corrected} = E_{original} - \rho \times A$, where the corrected EM-jet energy is $E_{corrected}$, and the original EM-jet energy is $E_{original}$.

Figure (4.1) shows the UE correction distribution for EM-jet energy. The left plot shows the subtraction term for the UE correction for EM-jet energy. The right plot shows the EM-jet energy distribution after the UE correction. If the EM-jet energy after subtraction is less than 0 GeV, the energy will be set to 0 GeV.

4.2 Detector level to particle level EM-jet energy correction

The EM-jet energy obtained from FMS is considered detector-level EM-jet energy. Therefore, a correction for detector level to particle level EM-jet energy is necessary. The correction is based on the Monte Carlo simulation for FMS. For

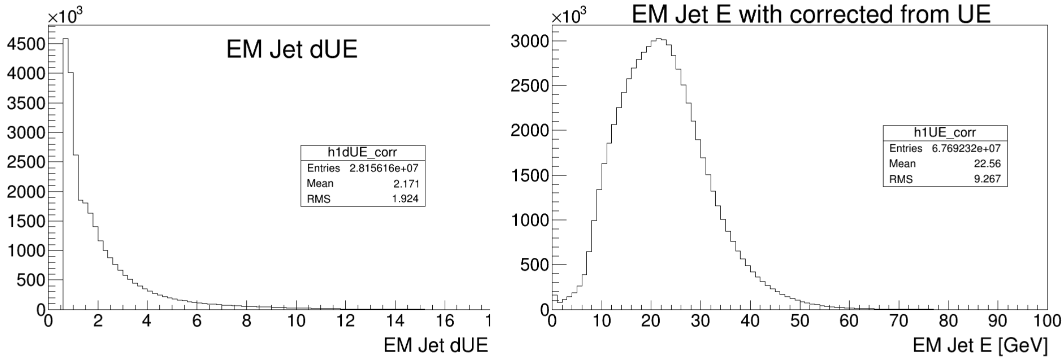

Figure 4.1: UE distribution for diffractive EM-jet analysis. The left plot shows the subtraction term $\rho \times A$. The right plot shows the EM-jet energy distribution after the UE correction.

the PYTHIA simulation, the proton-proton collisions with $\sqrt{s} = 200$ GeV are generated, with the tune setting of Perugia2012 (Tune parameter 370) [18, 19]. Then, the GEANT3 with FMS detector response implemented under STAR simulation framework ("starsim") is used for the FMS simulation. The Big Full Chain (BFC) proceeds with the event reconstruction. The chain options are "ry2015a agml usexgeom MakeEvent McEvent vfmce Idst BAna l0 l3 Tree logger fmsSim fmspoint evout -dstout IdTruth bigbig fzin geantout clearmem sdt20150417.193427". The EM-jet reconstruction is proceeded along with the BFC process. The Anti-k_T algorithm with R=0.7 is used for the EM-jet reconstruction, the same as the EM-jet reconstruction for data.

For the simulation results, the EM-jets with both particle level and detector level are recorded. Figure (4.2) shows the EM-jet energy distribution in particle level (y-axis) and detector level (x-axis). Figure (4.3) shows the profile of the EM-jet energy distribution with particle level and detector level. The black points are the correlation between the EM-jet energy at the particle level and detector level. The red curves are fit for the points in two different detector level regions: $5 < E < 10$ GeV and $10 < E < 60$ GeV. The 6th-order polynomial function is used for fitting the former region and the linear function is used for fitting the latter region. The parameters of the 6th-order polynomial are shown in Tab. (4.1), while the linear function is: $E_{par} = 1.07 * E_{det} + 1.13$, where E_{par} is the particle level EM-jet energy and E_{det} is the detector level EM-jet energy. These functions are used to calculate the corrected energy from the original detector level energy. The corrected EM-jet energy will finally applied for the x_F calculation and A_N extraction.

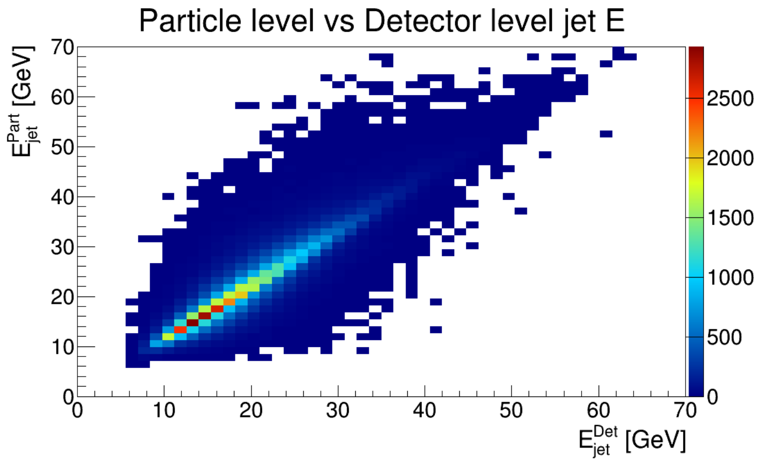

Figure 4.2: EM-jet energy distribution in particle level (y-axis) and detector level (x-axis) from the FMS simulation.

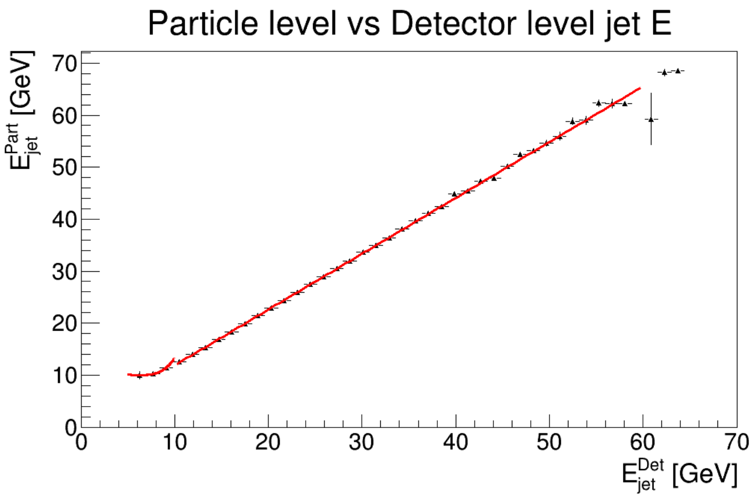

Figure 4.3: The profile of the EM-jet energy distribution with particle level and detector level. The black points are the correlation between the EM-jet energy at the particle level and detector level. The red curves are the fit for the black points.

[0]	[1]	[2]	[3]	[4]	[5]	[6]
8.93e0	-6.64e-1	1.51e-1	-6.66e-3	1.56e-4	-1.85e-6	8.65e-9

Table 4.1: Parameters for the 6th-order polynomial

Chapter 5

Rapidity Gap (RG) events study

5.1 Motivation

The rapidity gap (RG) events are also within our interest in studying the potential background for the single diffractive events. The RG events are the type of events coinciding with FMS EM-jets and East BBC veto. The details description for the FMS EM-jets and east BBC veto are in Sec. (5.2). Since there is no requirement on the RP track (proton) on any side, the RG events are considered as the subset of the inclusive events, and they can also serve as additional enrichment for the inclusive process. According to the Pythia 8 simulation for hard QCD process (can be considered as non-single diffractive events) and the single diffractive events, the east BBC veto cuts are able to cut out about 84% of the non-single diffractive events, but just cut out about 14% of the single diffractive events with a proton on the east side. Therefore, such a process can help separate the diffractive and non-diffractive processes with the rapidity gap requirement. Studying the RG events can allow us to investigate the single diffractive process without the effects on the limited Roman Pot acceptance for tagging the scattered proton.

5.2 Event selection for RG events

The dataset used for the RG events is the same as single diffractive events, shown in Sec. (2.1). The event selection criteria of the FMS EM-jets, event property cuts, and the East BBC veto for the RG events are the same as those for the single diffractive events, which are shown in Sec. (3.1), Sec. (3.2) and

Sec. (3.3), respectively. The idea behind choosing the same FMS EM-jet cuts and East BBC veto cuts is to make them consistent and comparable to the single diffractive process.

Chapter 6

Background study

6.1 Zerobias event study

The Zerobias events are the highly scaled events with the zerobias trigger. The details for the events are shown below:

- Trigger setup name: production_pp200trans_2015
- Data stream: zerobias
- Production tag: P16id

Since there are only a small fraction of events containing good EM-jets at the FMS, the Zerobias events are only used to estimate the accidental background for the analysis. To begin with, the NanoDst files are generated from the MuDst files. For the Zerobias events, there are no requirement on the EM-jets on FMS and no requirement on RP track. Then, the BBC East veto cuts (detailed in Sec. (3.3) and East RP track cuts (detailed in Sec. (3.4)) are applied to the Zerobias events, where both cuts are the same as single diffractive process. About 0.2% of the events pass the cuts mentioned above. Therefore, about 0.2% of the events are accidental coincidences and should be the same rate for every process.

With the Zerobias events, we also estimate the accidental coincidences (AC) for the measured single diffractive process. The AC events are coming from the situation that the FMS EM-jets and the east RP tracks are not correlated. For example, the FMS EM-jets and the east RP tracks are coming from multiple collisions, but they are recorded in one event in the data. Equation (6.1) shows the formula for calculating the fraction for the AC events. n_{AC} is the number of the AC events, but it is difficult to count directly. n_{mea} is the number of event counts per x_F bin in the asymmetry calculation for the single diffractive process. n_{RG} is the number of event counts per x_F bin in the asymmetry calculation for the RG events, where the description for RG events is in Sec. (5.1). $\frac{n_{AC}}{n_{RG}}$ can be considered as the AC events fraction for RG events, which is 0.2%. By counting the events per x_F bin for measured single diffractive process and RG events, the fraction for the AC events is about 1.8% for each x_F bin. This fraction is small, so its effect will be assigned to the systematic uncertainty, detailed in Appendix (A).

$$frac_{bkg} = \frac{n_{AC}}{n_{mea}} = \frac{n_{AC}}{n_{RG}} \times \frac{n_{RG}}{n_{mea}} \tag{6.1}$$

Chapter 7

Systematic Uncertainty

The systematic uncertainty for single diffractive process includes the cuts on East BBC veto cuts (details in 7.2), Ring of Fire (details in 7.3) and AC background (details in 6.1). However, The systematic uncertainty for rapidity gap events includes the cuts on East BBC veto cuts (details in 7.2) and Ring of Fire (details in 7.3).

7.1 Method for systematic uncertainty

To study the systematic uncertainty for the BBC East veto cuts and Ring of Fire, the Bayesian method is applied [21]. For each term of systematic uncertainty study, we calculate the A_N standard deviation among the variation cuts. However, only the cuts with variations deemed significant would be included. If a cut with variations produces a maximum value with statistical uncertainty $A_N(1) \pm \delta_1$ and a minimum value with statistical uncertainty $A_N(2) \pm \delta_2$, only when $\frac{|A_N(1)-A_N(2)|}{\sqrt{|\delta_1^2-\delta_2^2|}} > 1$ the standard variation will be used for this systematic uncertainty term, otherwise this systematic uncertainty term will be assigned 0 (Barlow check) [21]. All the systematic uncertainty for each x_F bin will be calculated individually.

7.2 Systematic uncertainty for the BBC East veto cuts

The BBC East veto cuts include East Large BBC ADC sum < 80 and East Small BBC ADC sum < 90. We change the cut values for East Large BBC and East Small BBC ADC sum to study the systematic uncertainty, as shown in Tab. (7.1). We calculate the A_N with its statistical uncertainty for each cut variation,

Variation	-20	-10	+10	+20
East Large BBC ADC sum cut	60	70	90	100
East Small BBC ADC sum cut	70	80	100	110

Table 7.1: List of East BBC veto cut values for systematic uncertainty study.

and only one variation is applied once. Also, the systematic uncertainty for East Large BBC and East Small BBC ADC sum cuts are studied separately.

7.3 Ring of Fire

The Ring of Fire is a kind of background related to the FMS-sm-bs3 trigger. This trigger is targeted at the inner region of FMS, which is close to the beam. It's generally recognized that the beam remnants are accepted by FMS-sm-bs3 trigger. Therefore, the effect of this trigger will be considered as one source of systematic uncertainty. The systematic uncertainty for the Ring of Fire will be the A_N result difference between considering this trigger and excluding this trigger. In addition, the Barlow check is applied to determine whether to keep the standard derivation as systematic uncertainty.

7.4 Polarization uncertainty

The blue beam and yellow beam polarization are used to calculate the A_N results. As a habit, the uncertainty of beam polarization uncertainty is listed independently. The beam polarization measurement results are provided by the CNI group, which develops, maintains, and operates the RHIC polarimeter measurement. The beam polarization measurement results are listed in the table on the webpage [22]. In the webpage, the starting time (t_0), the polarization of the blue (yellow) beam at the beginning of every fill (P_0), the decay rate ($\frac{dP}{dt}$) are provided for each fill. For each event, the beam polarization can be calculated from the time difference from the beginning of the fill using Equ. (7.1), where t_{event} is the time of each event. The beam polarization for each run can be calculated by Equ. (7.2), where t_{run} is the time of the center of the run. The beam polarization for each fill can be calculated using the weighted average run polarization with Equ. (7.3), where L_{run} is the luminosity of each run. However, since L_{run} is proportional to the number of events in each run, the number of events in each run will be replacing the luminosity of each run in the calculation.

$$P_{event} = P_0 + \frac{dP}{dt}(t_{event} - t_0) \tag{7.1}$$

$$P_{run} = P_0 + \frac{dP}{dt}(t_{run} - t_0) \tag{7.2}$$

$$P_{fill} = \frac{\sum_{run} L_{run} P_{run}}{\sum_{run} L_{run}} \tag{7.3}$$

The beam polarization uncertainty includes the scale uncertainty, fill-to-fill uncertainty, and uncertainty from the profile correction procedure [23].

The scale uncertainty is related to the polarization measurement methods. It includes H-jet scale, H-jet background and pC scale. For run 15, the scale uncertainty is 3% [23].

The relative uncertainty of the profiles correction for one beam in one fill is 2.2%. For a set of M fills, the relative profile correction for the single-spin asymmetry measurement is $\sigma(profile)/P = 2.2\%/\sqrt{M}$ [23]. For the run 15 FMS dataset, this uncertainty is about 0.3%.

The fill-to-fill uncertainty is propagated based on Equ. (7.3) with the uncertainty of P_0 and $\frac{dP}{dt}$. The uncertainty for these two terms $(\sigma(P_0))$ and $(\sigma(\frac{dP}{dt}))$ for either blue beam or yellow beam can be obtained in [22]. This uncertainty can be expressed in Equ. (7.4). The third term on the right side of the equation is due to the sensitivity of the measurement of the energy scale of the nuclei in the pC polarimetry [14], and it's negligible. However, for the term (Equ. (7.5)), this correction is overcounting for the measurement using a fraction of the run period. Therefore, a correction scale factor $\sqrt{1 - \frac{M}{N}}$ is applied for the second term, which is shown in Equ. (7.6). For this analysis, N=54 and M=142. The fill-to-fill uncertainty for single diffractive EM-jet analysis is about 0.3%.

$$\sigma^2(P_{fill}) = \sigma^2(P_0) + \sigma^2(\frac{dP}{dt}) \cdot (\frac{\sum_{run} t_{run} L_{run}}{L_{fill}} - t_0)^2 + (\frac{\sigma(fill - to - fill)}{P})^2 \cdot P_{fill}^2 \tag{7.4}$$

$$P_{set}^2 = (\frac{\sum_{run} t_{run} L_{run}}{L_{fill}}) \tag{7.5}$$

$$P_{fill-to-fill\ scale}^2 = (1 - \frac{N}{M}) \cdot P_{set}^2 \tag{7.6}$$

Finally, the polarization uncertainty is calculated in the quadrature. For the single diffractive EM-jet analysis, it's about 3%.

x_F	Small BBC east	Large BBC east	Ring of Fire	Background	Summary
0.2 - 0.25	0.0026	0.0041	0	0.0044	0.0064
0.25 - 0.3	0	0	0.0022	0.0034	0.0041
0.3 – 0.35	0	0.0020	0	0.0032	0.0037
0.35 – 0.4	0.0017	0.0034	0	0.0035	0.0052
0.4 – 0.45	0.0022	0.0052	0.012	0.0041	0.014

Table 7.2: Systematic uncertainty for blue beam A_N for all photon multiplicity EM-jets from single diffractive process

x_F	Small BBC east	Large BBC east	Ring of Fire	Background	Summary
0.2 - 0.25	0.0027	0.0054	0	0.0043	0.0074
0.25 - 0.3	0.0028	0.0025	0	0.0034	0.0051
0.3 – 0.35	0	0.0046	0	0.0031	0.0056
0.35 – 0.4	0.0018	0.0048	0.0051	0.0035	0.0080
0.4 – 0.45	0.0013	0.0022	0	0.0040	0.0048

Table 7.3: Systematic uncertainty for yellow beam A_N for all photon multiplicity EM-jets from single diffractive process

7.5 Summary for the systematic uncertainty

The final systematic uncertainty for single diffractive process and rapidity gap events will be counted bin by bin (x_F bin), and they are calculated as $\sqrt{\sum_i \sigma_i^2}$.

Table (7.2) and Table (7.3) show the systematic uncertainty for each and final term for the blue beam A_N and yellow beam A_N for all photon multiplicity EM-jets from single diffractive process, respectively. Table (7.4) and Table (7.5) show the systematic uncertainty for each and final term for the blue beam A_N and yellow beam A_N for one or two-photon multiplicity EM-jets from single diffractive process, respectively. Table (7.6) and Table (7.7) show the systematic uncertainty for each and final term for the blue beam A_N and yellow beam A_N for three or more photon multiplicity EM-jets from single diffractive process, respectively.

Also, table (7.8) and Table (7.9) show the systematic uncertainty for each and final term for the blue beam A_N and yellow beam A_N for all photon multiplicity EM-jets from rapidity gap events, respectively. Table (7.10) and Table (7.11) show the systematic uncertainty for each and final term for the blue beam A_N and yellow beam A_N for one or two-photon multiplicity EM-jets from rapidity gap events, respectively. Table (7.12) and Table (7.13) show the systematic uncertainty for each and final term for the blue beam A_N and yellow beam A_N for three or more photon multiplicity EM-jets from rapidity gap events, respectively.

x_F	Small BBC east	Large BBC east	Ring of Fire	Background	Summary
0.2 - 0.25	0.0040	0.0033	0	0.0057	0.0077
0.25 - 0.3	0.0024	0	0.0022	0.0046	0.0056
0.3 – 0.35	0.0018	0.0018	0	0.0044	0.0051
0.35 – 0.4	0.0032	0.0034	0	0.0047	0.0066
0.4 – 0.45	0.0055	0.0072	0.022	0.0052	0.024

Table 7.4: Systematic uncertainty for blue beam A_N for 1 or 2 photon multiplicity EM-jets from single diffractive process

x_F	Small BBC east	Large BBC east	Ring of Fire	Background	Summary
0.2 - 0.25	0.0035	0	0	0.0056	0.0065
0.25 - 0.3	0.0021	0.0035	0	0.0045	0.0061
0.3 – 0.35	0.0025	0.0041	0	0.0043	0.0064
0.35 – 0.4	0	0.0062	0	0.0046	0.0077
0.4 – 0.45	0.0016	0.0036	0.020	0.0052	0.021

Table 7.5: Systematic uncertainty for yellow beam A_N for 1 or 2 photon multiplicity EM-jets from single diffractive process

x_F	Small BBC east	Large BBC east	Ring of Fire	Background	Summary
0.2 - 0.25	0	0.0076	0	0.0068	0.010
0.25 - 0.3	0.0022	0.0028	0.0023	0.0051	0.0066
0.3 – 0.35	0	0	0	0.0046	0.0046
0.35 – 0.4	0	0.0047	0.0076	0.0055	0.010
0.4 – 0.45	0.0035	0.0053	0	0.0066	0.0091

Table 7.6: Systematic uncertainty for blue beam A_N for 3 or more photon multiplicity EM-jets from single diffractive process

x_F	Small BBC east	Large BBC east	Ring of Fire	Background	Summary
0.2 - 0.25	0.0098	0.014	0	0.0067	0.019
0.25 - 0.3	0.0037	0.0033	0	0.0046	0.0071
0.3 – 0.35	0.0030	0.0081	0.0046	0.0045	0.011
0.35 – 0.4	0.0037	0.0047	0.0051	0.0052	0.011
0.4 – 0.45	0	0	0.015	0.0065	0.017

Table 7.7: Systematic uncertainty for yellow beam A_N for 3 or more photon multiplicity EM-jets from single diffractive process

x_F	Small BBC east	Large BBC east	Ring of Fire	Summary
0.1 - 0.2	0	0.0064	0	0.0064
0.2 - 0.25	0.0016	0	0	0.0016
0.25 - 0.3	0.00051	0.00096	0.00042	0.0011
0.3 – 0.35	0.00084	0	0	0.00084
0.35 – 0.4	0.0014	0	0.0033	0.0036
0.4 – 0.45	0.0010	0.0011	0	0.0015

Table 7.8: Systematic uncertainty for blue beam A_N for all photon multiplicity EM-jets from rapidity gap events

x_F	Small BBC east	Large BBC east	Ring of Fire	Summary
0.1 - 0.2	0.0027	0	0	0.0027
0.2 - 0.25	0.00052	0.0019	0	0.0019
0.25 - 0.3	0.00064	0.0012	0	0.0013
0.3 − 0.35	0.00066	0.00047	0	0.00081
0.35 − 0.4	0.00092	0.0013	0.0023	0.0029
0.4 − 0.45	0	0.0012	0	0.0012

Table 7.9: Systematic uncertainty for yellow beam A_N for all photon multiplicity EM-jets from rapidity gap events

x_F	Small BBC east	Large BBC east	Ring of Fire	Summary
0.1 - 0.2	0.0028	0.0061	0	0.0067
0.2 - 0.25	0.0018	0.0019	0	0.0026
0.25 - 0.3	0	0	0.00070	0.00070
0.3 − 0.35	0.00094	0	0.0023	0.0025
0.35 − 0.4	0.0024	0.0017	0	0.0030
0.4 − 0.45	0.00074	0.0019	0	0.0020

Table 7.10: Systematic uncertainty for blue beam A_N for 1 or 2 photon multiplicity EM-jets from rapidity gap events

x_F	Small BBC east	Large BBC east	Ring of Fire	Summary
0.1 - 0.2	0.0027	0	0	0.0027
0.2 - 0.25	0.00081	0.0024	0	0.0018
0.25 - 0.3	0.0015	0.0011	0	0.0019
0.3 − 0.35	0.00086	0.0011	0.0017	0.0022
0.35 − 0.4	0	0.0015	0.0034	0.0037
0.4 − 0.45	0.00069	0	0.0059	0.0060

Table 7.11: Systematic uncertainty for yellow beam A_N for 1 or 2 photon multiplicity EM-jets from rapidity gap events

x_F	Small BBC east	Large BBC east	Ring of Fire	Summary
0.1 - 0.2	0	0.0088	0	0.0088
0.2 - 0.25	0.0015	0	0	0.0015
0.25 - 0.3	0	0	0	0
0.3 − 0.35	0.00082	0	0.0018	0.0020
0.35 − 0.4	0	0	0.0040	0.0040
0.4 − 0.45	0.0028	0.0021	0.0036	0.0050

Table 7.12: Systematic uncertainty for blue beam A_N for 3 or more photon multiplicity EM-jets from rapidity gap events

x_F	Small BBC east	Large BBC east	Ring of Fire	Summary
0.1 - 0.2	0.0045	0	0	0.0045
0.2 - 0.25	0	0.0028	0	0.0028
0.25 - 0.3	0.0014	0.0026	0	0.0029
0.3 – 0.35	0.0014	0	0	0.0014
0.35 – 0.4	0.0017	0.0014	0	0.0022
0.4 – 0.45	0.0017	0.0021	0.0046	0.0053

Table 7.13: Systematic uncertainty for yellow beam A_N for 3 or more photon multiplicity EM-jets from rapidity gap events

Chapter 8

Analysis Method and Results

8.1 A_N Extraction

The cross-ratio method is used to extract the A_N for single diffractive processes, and the corresponding formulas are shown in Equ. (8.1) and Equ. (8.2). In both equations, ϵ stands for the raw asymmetry. $N^{\uparrow(\downarrow)}(\phi)$, $N^{\uparrow(\downarrow)}(\phi+\pi)$ are the yields detected at ϕ, $(\phi+\pi)$ for spin up (down) state, where ϕ is the azimuthal angle of the EM-jet in the lab frame. In this analysis, the full 2π azimuthal coverage is split into 16 ranges. P is the average polarization of the proton beam, where the polarization for each event is calculated from Equ. (7.1). A cosine fit ($p_0\cos(\phi)+p_1$) is applied to extract the A_N from the raw asymmetry in Eq. (8.2), while the constant term p_1 could provide cross-check for possible unidentified asymmetry, but this analysis does not take it into account.

$$\epsilon = \frac{\sqrt{N^{\uparrow}(\phi)N^{\downarrow}(\phi+\pi)} - \sqrt{N^{\downarrow}(\phi)N^{\uparrow}(\phi+\pi)}}{\sqrt{N^{\uparrow}(\phi)N^{\downarrow}(\phi+\pi)} + \sqrt{N^{\downarrow}(\phi)N^{\uparrow}(\phi+\pi)}} \tag{8.1}$$

$$\epsilon = PA_N cos(\phi) \tag{8.2}$$

This method takes advantage of detector azimuthal symmetry and cancels effects due to the non-uniform detector efficiency and the time-dependent luminosity.

8.2 Single diffractive EM-jet A_N

Three cases of EM-jet are studied for A_N of the single diffractive process: the EM-jet with all photon multiplicity, with only one or two-photon multiplicity, and with three or more photon multiplicity. Figure (8.1) shows the preliminary plot for the single diffractive EM-jet A_N as a function of x_F for the three cases of photon multiplicity mentioned above. Among the three panels in the figure, the blue points are for the blue beam A_N, represented as $x_F > 0$, while the red points are for the yellow beam A_N, represented as $x_F < 0$. The top panel is the results for all photon multiplicity. The statistical uncertainty is shown in bar, while the systematic uncertainty is shown in shaded box. The 2.7 σ non-zero significance is observed for the blue beam A_N. The blue beam A_N for the EM-jets with one or two photon multiplicity case shows about 2.5 σ non-zero significance, showing in the middle panel. However, the blue beam A_N for the EM-jets with three or more photon multiplicity cases is consistent with zero. The EM-jet A_N for one or two-photon multiplicity case is larger than that for all photon multiplicity case and for three or more-photon multiplicity case, which is consistent with the results shown in the inclusive processes [24].

8.3 Rapidity gap events EM-jet A_N

For the A_N of the rapidity gap events, the same three cases of the EM-jet are explored: the EM-jet with all photon multiplicity, with only one or two-photon multiplicity, and with three or more photon multiplicity. Figure (8.2) shows the preliminary plot for the EM-jet A_N of the rapidity gap events as a function of x_F for the three cases of photon multiplicity mentioned above. The A_N of all photon multiplicity and one or two-photon multiplicity cases shows the non-zero value but with a similar scale as for the A_N of the inclusive process with the same two cases of photon multiplicity [24]. The A_N of the three or more photon multiplicity EM-jets shows to be consistent with zero. In addition, the yellow beam A_N is also consistent with zero, regardless of photon multiplicity.

Furthermore, to better visualize the A_N contributions of the single diffractive process and the rapidity gap events to the inclusive process, a direct comparison plot among the A_N for inclusive process, diffractive process, and rapidity gap events for one or two-photon multiplicity, and three or more-photon multiplicity are shown in Fig. (8.3). The A_N for the single diffractive process and the rapidity gap events are consistent with that for inclusive process within uncertainty coverage for most of the x_F regions for both multiplicity cases. The A_N for the three processes for EM-jets with three or more-photon multiplicity are all consistent with zero. These direct comparison results indicate that the single

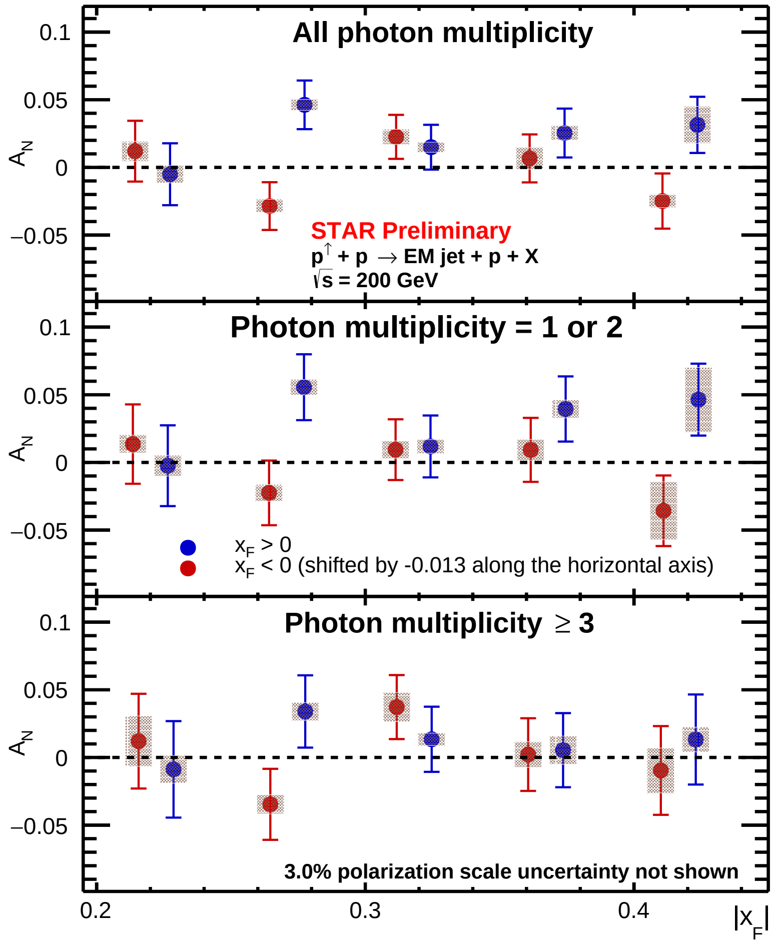

Figure 8.1: A_N for single diffractive events as a function of x_F for three different photon multiplicity cases: all photon multiplicity (top), one or two-photon multiplicity (middle), and three or more photon multiplicity (bottom). The A_N for $x_F < 0$ (red points) shifts -0.013 along the x-axis.

diffractive process can not provide evidence that it contributes to the large A_N in the inclusive process.

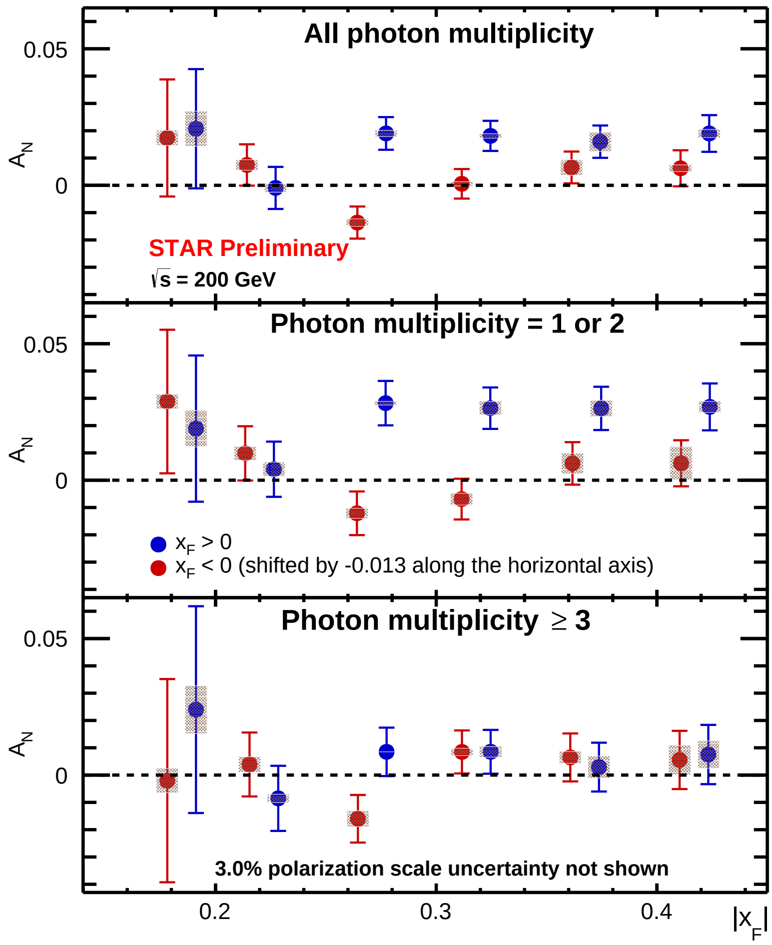

Figure 8.2: A_N for rapidity gap events as a function of x_F for three different photon multiplicity cases: all photon multiplicity (top), one or two-photon multiplicity (middle), and three or more photon multiplicity (bottom). The A_N for $x_F < 0$ (red points) shifts -0.013 along the x-axis.

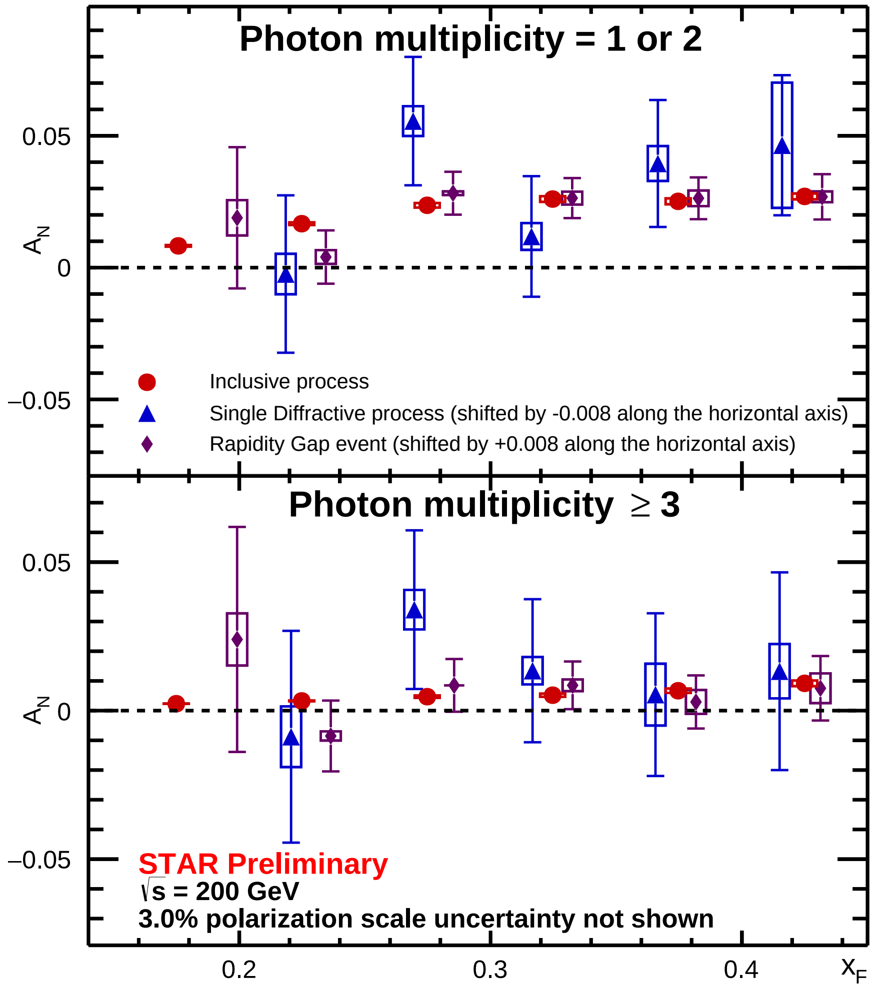

Figure 8.3: A_N for inclusive process (red), single diffractive process (blue), and the rapidity gap events (purple) as a function of x_F for one or two-photon multiplicity case (top panel) and three or more-photon multiplicity (bottom panel). The A_N for single diffractive process shifts -0.008 along the x-axis, and the A_N for rapidity gap events shifts +0.008 along the x-axis

Chapter 9

Conclusion

The transverse single-spin asymmetry as a function of EM-jet x_F from single diffractive process is explored. The all photon multiplicity and one or two-photon multiplicity EM-jet A_N for $x_F > 0$ from the single diffractive process show the non-zero values with more than 2-σ significance. In addition, the all photon multiplicity and one or two-photon multiplicity EM-jet A_N for $x_F > 0$ from the rapidity gap events show similar values as for inclusive process. The A_N for $x_F < 0$ from the single diffractive process and rapidity gap events are shown to be consistent with zero. Finally, comparing the one or two-photon multiplicity and three or more-photon multiplicity EM-jet among the inclusive process, the single diffractive process, and the rapidity gap events show their values are consistent within uncertainty. Therefore, no strong evidence exists that the single diffractive process will contribute to the large A_N in the inclusive process.

Appendix A

Derivation for the AC events effect to the uncertainty

The effect for the uncertainty in A_N calculation regarding the AC events is derived as follows. First of all, the corrected A_N is shown in Equ. (A.1). $A_N(sig)$ is the corrected A_N, while $A_N(mea)$ is the measured A_N which contains the effect of AC events. $frac(sig)$ is the signal fraction, while $frac(bkg)$ is the AC background fraction, which is about 1.8% (detailed in Sec. (6.1)). The error propagation for Equ. (A.1) is expressed in Equ. (A.2). Since the AC background fraction and its uncertainty are very small, the second and the third term are neglectable. Therefore, only the first term related to the statistical uncertainty of the measured asymmetry will be kept. The difference in the uncertainty between with and without the AC event correction will be assigned as systematic uncertainty.

$$A_N(sig) = \frac{A_N(mea) - frac(bkg) * A_N(bkg)}{frac(sig)} = \frac{A_N(mea) - frac(bkg) * A_N(bkg)}{1 - frac(bkg)} \tag{A.1}$$

$$
\begin{aligned}
\sigma^2 &= (\frac{\partial A_N(sig)}{\partial A_N(mea)})^2 \sigma A_N^2(mea) + (\frac{\partial A_N(sig)}{\partial frac(bkg)})^2 \sigma frac^2(bkg) + (\frac{\partial A_N(sig)}{\partial A_N(bkg)})^2 \sigma A_N^2(bkg) \\
&= (\frac{1}{1-frac(bkg)})^2 \sigma A_N^2(mea) + (\frac{A_N(sig)}{1-frac(bkg)})^2 \sigma frac^2(bkg) + (\frac{frac(bkg)}{1-frac(bkg)})^2 \sigma A_N^2(bkg) \\
&= (\frac{1}{frac(sig)})^2 \sigma A_N^2(mea) + (\frac{A_N(sig)}{frac(sig)})^2 \sigma frac^2(bkg) + (\frac{frac(bkg)}{frac(sig)})^2 \sigma A_N^2(bkg) \\
&\approx (\frac{1}{frac(sig)})^2 \sigma A_N^2(mea)
\end{aligned}
\tag{A.2}
$$

Bibliography

[1] D.L. Adams *et al.*, Phys. Lett. B 261, 201(1991)

[2] B.I. Abelev *et al.* (STAR Collaboration), Phys. Rev. Lett. 101, 222001(2008)

[3] A. Adare *et al.* Phys. Rev. D 90, 012006 (2014)

[4] E.C. Aschenauer *et al.*, arXiv:1602.03922

[5] J. Adam *et al.* (STAR Collaboration), Phys. Rev. D 103, 092009 (2021)

[6] G. L. Kane, J. Pumplin, and W. Repko. Phys. Rev. Lett. 41, 1689 (1978)

[7] D. Sivers, Phys. Rev. D 41, 83 (1990)

[8] J. Collins, Nucl Phys B 396 (1993) 161

[9] J.W. Qiu and G. Sterman, Phys. Rev. Lett. 67 2264 (1991)

[10] V. Khachatryan *et al.* (CMS Collaboration)

[11] M.M. Mondal (STAR Collaboration) PoS (DIS2014) 216 Phys. Rev. D 92, 012003 (2015)

[12] C. Kim, https://drupal.star.bnl.gov/STAR/starnotes/private/psn0735

[13] M.Cacciari, G. P. Salam, and G. Soyez, Eur. Phys. J. C (2012) 72: 1896

[14] Z. Zhu, https://drupal.star.bnl.gov/STAR/system/files/AnalysisNote_0601_0.pdf

[15] J. Adam *et al.* (STAR Collaboration), Results on Total and Elastic Cross Sections in Proton–Proton Collisions at $\sqrt{s} = 200$ GeV, Phys. Lett. B 808 (2020) 135663

[16] Particle Data Group, The review of particle physics, Prog. Theor. Exp. Phys. (2020) 083C01.

[17] B. B. Abelev *et al.* (ALICE Collaboration), Phys. Rev. D 91, 112012 (2015)

[18] T. Sjostrand, S. Mrenna, and P. Z. Skands, JHEP 05, 026 (2006)

[19] P. Skands, arXiv:1005.3457

[20] Peter Z. Skands Phys. Rev. D 82, 074018

[21] R. Barlow, Systematic Errors: facts and fictions, arXiv:hep-ex/0207026

[22] Run 15 polarization , https://wiki.bnl.gov/rhicspin/Run_15_polarization

[23] W. B. Schmidke, RHIC polarization for Runs 9-17 , Technical Report BNL-209057-2018- TECH, Brookhaven National Laboratory (2018)

[24] X. Liang (STAR Collaboration) 10.5281/zenodo.7236716